RSC Advances

PAPER

View Article Online
View Journal | View Issue

Check for updates

Cite this: *RSC Adv.*, 2025, **15**, 17015

Competitive growth kinetics of coexisting hydrogen bubbles on Ni electrodes: role of bubble nucleation density†

Weikang Yang, *[a] Dongxu Gu,[b] Xin Liu[a] and Qiangmin Luo[a]

The coverage of hydrogen bubbles decreases the active area of electrodes, resulting in reduced electrochemical performance. However, bubble growth locally decreases hydrogen concentration, thereby mitigating concentration overpotential. This dual effect highlights the significance of investigating the effect of bubbles on hydrogen removal in electrode design. Since hydrogen removal primarily occurs *via* molecular transport across bubble interfaces (which drives bubble growth), we analyzed the multi-bubble growth kinetics ($R = \alpha t^{\beta}$) on Ni electrodes with varying roughness to compare the hydrogen removal effect at the bubble interface. For a low-roughness (LR-surface) electrode, bubble growth follows conventional time coefficients (β) close to 0.5, indicating that the bubbles were in an H_2-saturated environment, where the entire bubble interface participated in hydrogen removal. The elevated bubble density on a medium-roughness (MR-surface) electrode provides additional bubble interfaces for hydrogen removal, reducing hydrogen concentration (α decrease from 93.91 to 63.11). The time coefficient of bubble growth remained at 0.5, confirming that the increased bubble interface was also in the hydrogen-saturated condition. In contrast, on a high-roughness (HR-surface) electrode, the competition of excessive coexisting bubbles for hydrogen molecules leads to the narrowing of the H_2-saturated region, and the top of the bubble is in the H_2-unsaturated region, indicating that not all of the additional bubble interface is involved in the hydrogen removal, which is manifested as the decrease in the time coefficient (β decrease from 0.5 to 0.42). Based on the experimental results, we conclude that the hydrogen removal effect does not increase linearly with increasing numbers of coexisting bubbles on the electrode. The transition in bubble growth kinetics reflects the varying degree of bubble interface involvement in hydrogen removal, which may serve as a consideration for designing the density of bubble nucleation sites on electrodes.

Received 28th March 2025
Accepted 5th May 2025

DOI: 10.1039/d5ra02159f

rsc.li/rsc-advances

Open Access Article. Published on 21 May 2025. Downloaded on 6/14/2026 1:50:35 PM.
This article is licensed under a Creative Commons Attribution-NonCommercial 3.0 Unported Licence.

1. Introduction

Electrolytic hydrogen production is considered one of the most promising approaches to address future energy crises.[1–8] Presently, extensive efforts are being undertaken to develop catalysts with high intrinsic activity to reduce the energy barrier for water splitting.[9–12] However, the substantial impact of hydrogen (H_2) bubbles adhering to the electrode has historically been overlooked. Many studies have highlighted that growing bubbles can obscure the catalyst surface, resulting in a reduction in the active area of the electrode.[13–18] This phenomenon also induces undesired ohmic overpotential, resulting in energy loss and efficiency degradation.[19–25] However, bubble growth originates from the mass transfer of hydrogen molecules in the electrolyte, which reduces local hydrogen concentration near the electrode and consequently mitigates concentration overpotential effects. Therefore, achieving an optimal balance between these dual bubble effects is critical for hydrogen evolution electrode design. Specifically, we aim for full bubble interfacial participation in hydrogen removal.

The removal of hydrogen molecules by bubbles primarily occurs through mass transfer across the gas–liquid interface into the bubbles. We therefore characterized the multi-bubble growth kinetics on nickel (Ni) electrodes to evaluate the hydrogen removal efficiency at bubble interfaces. According to previous experimental and simulation studies, the bubble growth follows a power-law behavior, which can be described as $R(t) = \alpha t^{\beta}$, where α represents the growth coefficient and β denotes the time coefficient.[26–32] The time coefficient of bubbles is fundamentally governed by the diffusion process of hydrogen molecules from the surrounding environment into the bubble. Wang *et al.*[28] employed two distinct approaches to modulate the effective electrode area of TiO_2 photoanodes: (1)

[a]*School of Chemistry and Chemical Engineering, Chongqing University, Chongqing 400044, PR China. E-mail: wkyang@stu.cqu.edu.cn; Tel: +86 18725737346*

[b]*Institute of Intelligent Innovation, Henan Academy of Sciences, Zhengzhou, Henan, 451162, P. R. China*

† Electronic supplementary information (ESI) available. See DOI: https://doi.org/10.1039/d5ra02159f

© 2025 The Author(s). Published by the Royal Society of Chemistry

Open Access Article. Published on 21 May 2025. Downloaded on 6/14/2026 1:50:35 PM.
This article is licensed under a Creative Commons Attribution-NonCommercial 3.0 Unported Licence.

full-electrode (3 cm^2) electrochemical gas evolution; (2) laser-localized irradiation (0.00785 cm^2) for photoelectrochemical gas generation, observing two distinct time coefficients (β). The experimental results reveal that when bubbles are significantly smaller than the electrode's reactive area, they reside in a gas-saturated environment where growth is limited by molecular diffusion across the gas–liquid interface ($\beta = 0.5$), with the entire bubble interface participating in hydrogen removal. Conversely, when the effective electrode area was reduced, the bubble's time coefficient significantly decreased to 0.33, as gas molecules generated at the electrode directly entered the bubble, limiting the process reaction, and most of the bubble's interface remained inactive during hydrogen removal. Bashkatov *et al.*[30] presented additional experimental evidence by investigating single hydrogen bubble growth on Pt microelectrodes in H_2SO_4 electrolyte. Their results demonstrated a time coefficient evolution of the bubble growth: an initial $\beta = 0.5$ for several milliseconds, followed by a transition to a stable $\beta = 0.33$, when the bubble dimensions exceeded the size of the microelectrode. These results show that the degree of bubble interface participation in hydrogen removal can be reflected in bubble growth kinetics. During the actual water electrolysis, multiple bubbles grow simultaneously on the electrode but are not isolated. Therefore, it is valuable to investigate the effects of other coexisting bubbles on the bubble growth kinetics of electrodes.

In this study, we investigated the growth kinetics of multiple coexisting bubbles on the electrode surface. We also performed the hydrogen evolution reaction (HER) as a probe reaction on a Ni electrode, whose bubble nucleation density was well controlled by altering the surface roughness of the electrode. The experimental results show that the influence of coexisting bubbles on the bubble growth kinetics is obvious. The bubble growth rate decreases with the increase in the number of coexisting bubbles on the electrode, which is reflected by the decrease in the growth coefficient (α) in the form of $R(t) = \alpha t^{\beta}$. Upon reaching a certain critical density of nucleation sites, the bubble growth changed from a diffusion-limited to a concentration-limited pattern, as manifested by a decrease in the time coefficient (β). The experimental results demonstrate that excessive coexisting bubble competition for hydrogen molecules induces a narrowing of the diffusion boundary layer, resulting in hydrogen-undersaturated conditions at the bubble top regions. This phenomenon fundamentally indicates the existence of an optimal upper limit for the density of bubble nucleation sites.

2. Experimental

2.1 Experimental setup

The Ni electrodes were prepared based on previously reported methods.[33] In summary, the Ni block was encapsulated with epoxy resin to expose only the working face (∅ 5 mm). The subsequent working face was directly polished using sandpaper (wuxi-1200, wuxi-800 and wuxi-400) to prepare three representative Ni electrodes with a low roughness surface (LR-surface), a medium roughness surface (MR-surface), and a high roughness surface (HR-surface), which were utilized as working electrodes. The experimental setup is shown in Fig. 1, where the working face of the Ni electrode faces the high-speed camera to enable clear observation of the hydrogen evolution process on the Ni electrodes. The LED was on the same side as the high-speed camera to use the reflected light from the electrode for imaging. The hydrogen bubbles could be imaged under the lens and showed a clear dark coloration.

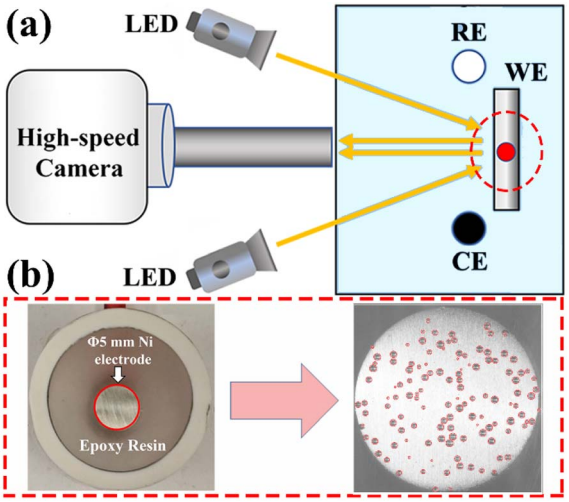

Fig. 1 (a) Experimental setup, (b) Ni electrode and typical images obtained using a high-speed camera.

2.2 Electrochemical measurements

All electrochemical measurements were performed using a CHI660C electrochemical workstation (Shanghai Chenhua Instruments Inc., China). The Standard three-electrode configuration was employed, consisting of a carbon rod counter electrode and an Hg/Hg_2SO_4 reference electrode, along with a Ni electrode (working electrode). The electrodes were assembled in a quartz glass cell (5 × 5 × 10 cm^3) with an electrolyte of 0.5 M H_2SO_4 solution (Kelong Chemical Reagents Co., Ltd, China). Cyclic voltammetry (CV) measurements were carried out in non-faradaic regions (open-circuit potential ±50 mV), employing various scan rates ranging from 25 to 500 mV s^{-1} to evaluate the electrochemically active surface area (ECSA). The chronopotentiometry method was employed to investigate the bubble growth kinetics. In our experiments, the current density was kept consistent across all samples to maintain a uniform hydrogen production rate. HER was conducted at a relatively low current density of 2.5 mA cm^{-2} to prevent excessive bubble formation that could interfere with observations.

2.3 Characterization

The morphology of the electrodes was observed using a material microscope (LEICA DM4000M, Germany). The differences in the wettability of the electrodes with varying levels of roughness were evaluated using a contact-angle meter (Dataphysics OCA20, Germany). The height of the electrode surfaces was calculated using an MFP-3D Origin atomic force microscope

© 2025 The Author(s). Published by the Royal Society of Chemistry

Open Access Article. Published on 21 May 2025. Downloaded on 6/14/2026 1:50:35 PM.
This article is licensed under a Creative Commons Attribution-NonCommercial 3.0 Unported Licence.

(AFM, Oxford Instruments, USA). The root mean square value of the height at all positions (R_q) was used to quantitatively describe the roughness of the electrode surface.

2.4 Visualization and image analysis

The growth and detachment of the bubbles were recorded under high-power LED illumination (Aputure 300d II, China) using a high-speed camera (Phantom VEO-E 310L, USA). The optical axis of the camera was perpendicular to the electrode surface (Fig. 1). The exposure time and frame rate of the camera were set to 0.1 ms and 100 fps, respectively. The sampled image was captured from a top view of the electrode surface at a resolution of the image is 1280 × 800 pixels. For the analysis of bubble images on the electrode, we developed a program utilizing the image processing module of MATLAB (R 2022b) to digitize the captured images and extract parameters of bubble size (More details shown in the ESI†). To obtain the true size, we must perform pixel calibration of the image. We captured an image of a calibration scale with a minimum graduation of 100 μm. The pixel scale (μm per pixel) was then calculated as $100/d$, where d represents the pixel length corresponding to the minimum division. The magnification ratio of high-speed photography can influence actual scale measurements. Therefore, after calibration, the magnification setting was maintained constant throughout the experiments. The narrow field depth characteristics of high-speed cameras exert negligible influence on the measurement accuracy when a proper focus is achieved.

The bubble size was determined through the following steps: (1) background subtraction, noise filtering, binarization, and hole filling; (2) utilization of the Hough algorithm to identify multiple bubbles in the pre-processed images. Upon bubble identification, geometric parameters were recorded. By iterating through steps (1) and (2) for all frames of the video, we obtain continuous size changes of multiple bubbles on the electrode in the time domain. The growth kinetics of the five bubbles on each electrode were collected to ensure the reliability of the experiment.

3. Results and discussion

3.1 Characterization

The surface morphology of the fabricated Ni electrodes was characterized using a material microscope, revealing pronounced differences in surface topography among the electrodes with varying levels of roughness. As illustrated in Fig. 2a, the high-roughness (HR-surface) electrode exhibited numerous pits attributed to the larger particles present in the low mesh sandpaper. These pits were uniformly distributed across the electrode, resulting in a surface topography with large height variations and pronounced roughness. The medium-roughness (MR-surface) and low-roughness (LR-surface) electrodes are shown in Fig. 2b and c, respectively. With the use of high-mesh sandpaper during the preparation process, the pits with substantial height variations gradually diminished until they were no longer visible. On the MR-surface electrode (Fig. 2b), faint stripes were discernible because of the

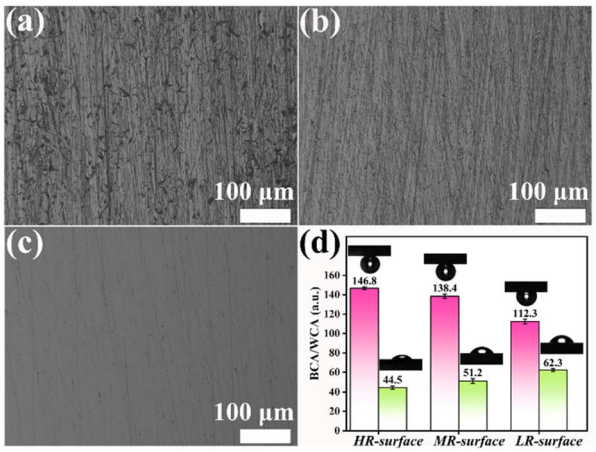

Fig. 2 (a) Surface morphology of the HR-surface electrode, (b) surface morphology of the MR-surface electrode, (c) surface morphology of the LR-surface electrode, (d) histogram of the contact angle of droplet/bubble on the electrodes, with a snapshot at the top (pink: the bubble contact angle and cyan: the droplet contact angle).

sandpaper treatment process, indicating a notable reduction in roughness. As shown in Fig. 2c, the LR-surface electrode exhibited a smooth surface with only minimal incidental traces, indicating the attainment of low roughness on the fabricated electrode surface. The electrodes with different levels of roughness induce variations in surface wettability.[34,35] As shown in Fig. 2d, the contact angle of water droplets on HR-surface, MR-surface, and LR-surface electrodes increased from 44.5° to 51.2° and 62.3°, respectively, while the contact angle of underwater bubbles decreased from 146.8° to 138.4° and 112.3°, respectively. The results indicated that for Ni electrodes, as the surface roughness increased, the hydrophilicity of the Ni electrode surface also increased, and the interaction between bubbles and the electrode surfaces decreased. Furthermore, the interaction between the bubbles and the electrodes was evaluated using a bubble probe constructed using AFM (More details shown in ESI†). As presented in Table S1,† the adhesion of bubbles to the LR-surface, MR-surface and HR-surface electrodes decreased from 3.74 nN to 1.82 nN and 1.12 nN, respectively, based on the characterization of the bubble contact angles. The measured adhesion forces were significantly lower than the theoretical pinning forces calculated from the surface tension principles. We attribute this discrepancy to two primary factors: first, during the pressing phase, the bubble may not have fully reached its equilibrium wetting state before detachment was initiated. Second, the bubbles maintained a Cassie–Baxter state on the rough electrode surface, where discrete solid–liquid contact points rather than continuous contact lines formed, leading to substantially reduced effective contact lengths for pinning. Although the absolute values are significantly lower than the theoretical predictions, they serve as meaningful qualitative indicators of comparative analysis.

The roughness of the fabricated Ni electrodes was compared by determining their roughness factor, which was indirectly estimated by identifying the electrical double-layer capacitance of the Ni electrodes.[36] Cyclic voltammetry near the open-circuit

Open Access Article. Published on 21 May 2025. Downloaded on 6/14/2026 1:50:35 PM.
This article is licensed under a Creative Commons Attribution-NonCommercial 3.0 Unported Licence.

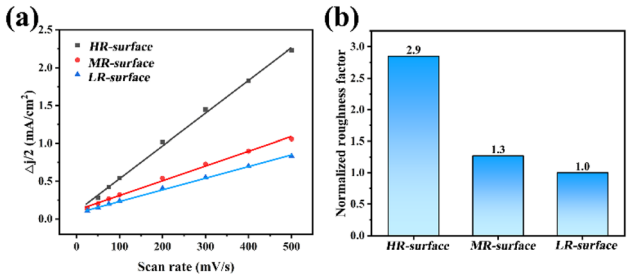

Fig. 3 (a) Cyclic voltammetry results at various scanning speeds. (b) Roughness factors of the three electrodes.

voltage (Fig. S3†), with a voltage range of 50 mV, was employed for each Ni electrode to obtain its double-layer capacitance at various scanning speeds (Fig. 3a). Subsequently, the roughness factors of the three electrodes were obtained by normalizing the LR-surface electrode, as shown in Fig. 3b. The roughness factor of the electrodes gradually decreased, demonstrating that Ni electrodes with three levels of roughness were successfully prepared.

To obtain a finer-scale morphology of the electrode surface and quantify the roughness, atomic force microscopy was employed to capture the topography of the prepared Ni electrode surface. As shown in Fig. 4a–c, the three-dimensional surface morphology of the Ni electrodes exhibited ridge-like features, which were associated with the surface treatment of the electrodes. The HR-surface electrode exhibited prominent ridge-like structures with the largest height variations. The height variations of the MR-surface electrode were reduced, while the LR-surface electrode demonstrated the smoothest surface among the three, consistent with the observations of the material microscopy. To effectively illustrate the overall surface features, the two-dimensional surface morphology of the three Ni electrodes is shown in Fig. 4d–f. In these depictions, the lighter color indicates higher elevations on the electrode surface. Subsequently, we sampled the height variations of the electrode, and the sampling path is indicated by a red line. The plotted height variation distributions are shown in Fig. 4g–i.

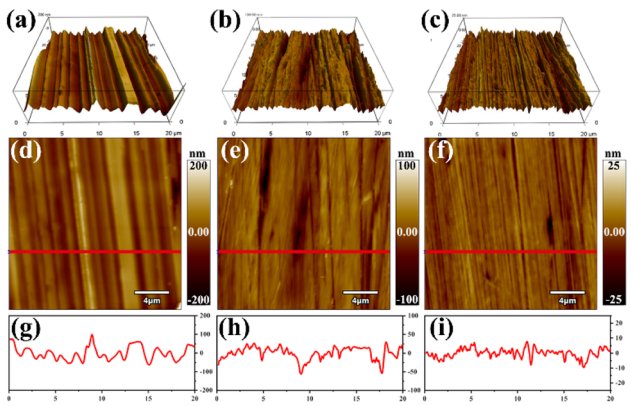

Fig. 4 (a–c) Three-dimensional surface morphology of the Ni electrodes. (d–f) Two-dimensional surface morphology of the three Ni electrodes. (g–i) Height variation distribution of the red lines in (d–f).

Table 1 The roughness (R_q) of the Ni electrodes[a]

Sample	Mean of R_q (nm)	Range of R_q (nm)	SD-R_q (nm)
HR-surface	42.44	26.01	9.19
MR-surface	16.37	9.11	3.40
LR-surface	3.69	1.34	0.43

[a] SD: standard deviation.

Within the sampled region, the HR-surface electrode showed a large drop (161 nm), followed by the MR-surface electrode, and the LR-surface electrode had a remarkably smooth surface, with negligible height variations of only 17 nm. In the present experiments, three parallel Ni electrodes were fabricated under identical preparation conditions. Three random regions were selected and measured for each sample using AFM. The measurement region size was 20 × 20 μm to ensure consistency, and the average roughness was calculated to minimize experimental errors. The statistical results are presented in Table 1.

3.2 Kinetics of the multiple bubbles

During the electrolysis process, the growth of hydrogen bubbles on the electrode surface is determined by the rate of hydrogen molecule generation from the faradaic reaction ($2H^+ + 2e^- \rightarrow H_2$) and the rate of hydrogen molecule diffusion in the electrolyte.[37] It is worth noting that the working face of the Ni electrodes used in our experiment had a circular shape with a diameter of 500 μm. The larger working face facilitated the simultaneous growth of multiple bubbles on the electrodes, which is different from the majority of previously reported research on bubble growth kinetics.[29,30,32] Fig. 5a–c illustrates the hydrogen bubbles on the HR-surface, MR-surface, and LR-surface electrodes, respectively. The frames represent a single snapshot captured from the recorded videos, revealing

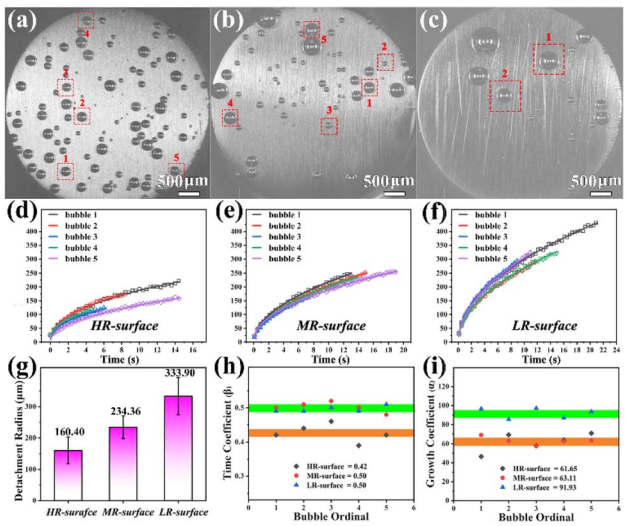

Fig. 5 (a–c) Frames of coexisting hydrogen bubbles on the Ni electrodes. (d–f) Kinetics of bubble growth on the Ni electrodes. (g) Average detachment size of bubbles on the Ni electrodes. (h) Average time coefficient of bubbles on the Ni electrodes. (i) Average growth coefficient of bubbles on the Ni electrodes.

© 2025 The Author(s). Published by the Royal Society of Chemistry

Open Access Article. Published on 21 May 2025. Downloaded on 6/14/2026 1:50:35 PM.
This article is licensed under a Creative Commons Attribution-NonCommercial 3.0 Unported Licence.

a stepwise decrease in the number of bubbles on the electrodes with varying roughness levels. In Fig. 5a, the HR-surface electrode exhibited several coexisting bubbles, which were attributed to its complex surface structure and the low degree of supersaturation required for bubble nucleation.[38] As shown in Fig. 5b, the MR-surface electrode exhibited a decreased number of simultaneously existing bubbles on the electrode. This reduction can be attributed to the diminution of surface height variation and roughness of the electrode. On the LR-surface electrode (Fig. 5c), only a small amount of coexisting bubbles was observed, which could be attributed to the smoothing of the electrode surface, requiring a larger supersaturation for bubble precipitation on the surface. To quantitatively describe the kinetics, typical bubble growth processes were then obtained by image processing to track the variation of the bubble radius over time. To ensure the reliability of the experiment, five bubbles were randomly selected and analyzed on each electrode to determine their growth kinetic parameters. The selected bubbles are highlighted by red boxes in Fig. 5a–c. It is essential to emphasize that the coexistence of multiple bubbles was challenging to observe on the LR-surface electrode, due to a low nucleation site density of bubbles. Therefore, five bubbles from the LR-surface electrodes cannot be highlighted in one frame (Fig. 5c). The typical time-dependent bubble growth kinetics on each electrode are shown in Fig. 5d–f. Through observation of the individual bubble growth process, it was found that the evolution kinetics of bubbles on the electrode all exhibit power-law behavior ($R = \alpha t^{\beta}$), where the time coefficient was closely related to the growth kinetics of the bubbles. As shown in Fig. 5g, the average detachment size of the bubbles on the HR-surface electrode was 160.40 μm, smaller than those on the MR-surface and LR-surface electrodes, which can be attributed to the difference in adhesion forces between the bubbles and the electrodes, which is consistent with the trends reported in the literature. Unexpectedly, as shown in Fig. 5h, the bubbles on the HR-surface electrode exhibited the smallest time coefficient (0.42), while the typical time coefficient for bubbles on the MR-surface and LR-surface electrodes was close to 0.50. The difference in the time coefficients indicates a transition in the bubble growth kinetics from diffusion-limited to concentration-limited, thereby extending the period for the bubbles to reach detachment size. Fig. 5i illustrates the bubble growth coefficients on different electrodes. Under the same growth kinetics of bubbles for the LR-surface and MR-surface electrodes, the decrease in the growth coefficient suggests a lower level of oversaturation on the MR-surface, which is attributed to the rapid decrease in hydrogen molecule oversaturation caused by more nucleation and growth of bubbles. It is worth noting that with more bubbles, the growth kinetics of the bubbles on the HR-surface electrode change, rather than their growth coefficient decreasing.

3.3 Mechanism discussion

The above results indicated a close relationship between the bubble kinetics and the surface roughness of the electrode. After the nucleation of the bubbles, the subsequent growth process is determined by the reaction rate of the electrode, the gas transfer, and the adsorption and desorption rates of hydrogen molecules at the bubble interface, as shown in Fig. 6a.[39] First, hydrogen molecules generated by the chemical reaction on the electrode surface continuously dissolve in the vicinity of the electrode surface. Through the competition between the adsorption and desorption of hydrogen molecules at the gas–liquid interface, hydrogen molecules diffuse into the interface, causing bubble growth.

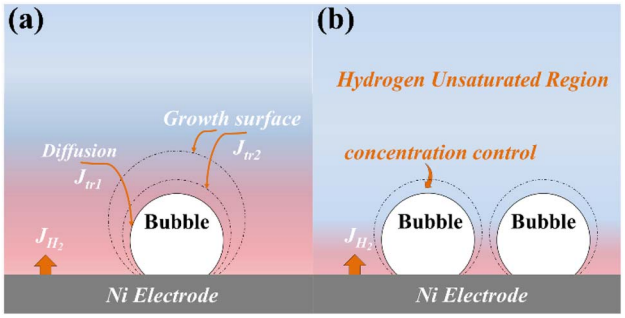

Fig. 6 (a) Growth process of hydrogen bubbles on Ni electrodes. (b) Growth process of multiple bubbles coexisting on Ni electrodes.

Assuming that the bubbles pinned on the electrode were spherical, the mass flux of hydrogen molecules entering the bubbles can be expressed as follows:

$$J_{\mathrm{gas}} = \frac{\mathrm{d}}{\mathrm{d}t}\left(\frac{V}{V_{\mathrm{m}}}\right) = \frac{\mathrm{d}}{\mathrm{d}t}\left(\frac{4\pi R^3}{3V_{\mathrm{m}}}\right) \quad (1)$$

where V_{m} ($\mathrm{m^3\ mol^{-1}}$) is the molar volume of hydrogen. If bubbles grow under a concentration-limited pattern, then the concentration of hydrogen molecules in the liquid becomes the rate-limiting step for bubble growth; that is, the reaction flux (J_{r}) of hydrogen molecules on the electrode surface limits bubble growth ($J_{\mathrm{r}} = J_{\mathrm{gas}}$). Therefore, bubble kinetics with a time coefficient $\beta = 0.3$ could be obtained as follows:[40]

$$R(t) = \left(\frac{3V_{\mathrm{m}}J_{\mathrm{r}}}{4\pi}\right)^{1/3} t^{1/3} \quad (2)$$

When the bubble growth occurs under a diffusion-limited pattern, the bubble growth rate J_{gas} ($\mathrm{mol\ s^{-1}}$) is equal to the transfer rate of gas molecules to the bubble interface J_{tr}. It should be noted that the hydrogen outflow flux is considered negligible when the bubbles are completely immersed in a hydrogen-saturated environment. The transfer rate of gas molecules is determined by two crucial factors: the molecular diffusion flux J_{tr1}, which is caused by the concentration gradient of gas molecules, and the micro-convection flux J_{tr2} driven by the expansion of the gas–liquid interface. The total diffusion flux to the bubble interface can be described as follows:[41]

$$J_{\mathrm{tr}} = J_{\mathrm{tr1}} + J_{\mathrm{tr2}} = S_{\mathrm{b}}D\left(\frac{1}{R} - \sqrt{\frac{2}{RD}\frac{\mathrm{d}R}{\mathrm{d}t}}\right)(C_l - C_i) \quad (3)$$

where S_{b} denotes the interface area of the bubble, D represents the diffusion coefficient of Hydrogen in the liquid, C_{l} and C_{i} are

Open Access Article. Published on 21 May 2025. Downloaded on 6/14/2026 1:50:35 PM.
This article is licensed under a Creative Commons Attribution-NonCommercial 3.0 Unported Licence.

the hydrogen concentrations in the liquid and at the bubble interface, respectively. Combined with eqn (1), the following equation with a time coefficient $\beta = 0.5$ can be obtained:

$$R(t) = \gamma t^{1/2} \quad (4)$$

where $\gamma = \sqrt{D}(A + \sqrt{A^2 + 2A})$, and $A = V_m (C_l - C_i)$.[32]

The bubble growth law equations provide two mathematical models of the bubble growth mechanism controlled by the concentration and diffusion of hydrogen molecules, respectively.

In our experiment, the growth of bubbles on the HR-surface electrode fell between the diffusion-limited pattern and the concentration-limited pattern with a time coefficient of only 0.42 (Fig. 5d). This indicates that the concentration of hydrogen molecules in the bubble environment is a major factor limiting the rapid growth. The growth of bubbles on the LR-surface and MR-surface electrodes consistently exhibits a diffusion-limited pattern with a time coefficient close to 0.5. Although there was a decrease in the growth coefficient on the MR-surface electrode, the time coefficient indicates that the rate of hydrogen molecule production at the electrode exceeds the rate of diffusion into the bubble and does not restrict the growth of the bubbles, as shown in Fig. 5e and f. Based on the experimental results, we believe that there may be a mismatch between the nucleation of bubbles and subsequent growth on the electrode. Specifically, an increase in the surface roughness of the electrode may lead to over-nucleated bubbles. As shown in Fig. 6b, the top of the bubble resides in an unsaturated region of hydrogen molecules due to excessive bubbles on the electrode, which significantly impedes bubble growth and elongates the time for the bubble to reach detachment size.

4. Conclusions

In summary, we fabricated three Ni electrodes with different roughness levels and investigated the growth kinetics of multiple hydrogen bubbles coexisting on the electrodes. The experiment revealed that the increase in electrode roughness changed the bubble growth kinetics due to excess bubble nucleation on the rough surface. The least nucleating bubbles were formed on the LR-surface electrode, resulting in bubble growth in a diffusion control mode, and the bubble interface was involved in the removal of hydrogen molecules. The MR-surface electrode exhibited an increased number of bubbles, inducing competition among multiple bubbles for hydrogen molecules. Therefore, the growth coefficient of each bubble decreased (from 93.91 to 63.11), yet they continued to grow in a diffusion-controlled pattern, indicating that the increased bubble surface was also involved in the removal of hydrogen molecules. On the HR-surface electrodes, excessive bubble nucleation resulted in an insufficient supply of hydrogen molecules to the electrode. Consequently, the growth of the bubbles was limited by the concentration of surrounding hydrogen molecules, prompting a transition in the growth kinetics from diffusion control to concentration control ($\beta = 0.42$), which indicates that the top region of the bubble is in an environment of unsaturated hydrogen molecules, and the bubble interface does not fully participate in the removal of hydrogen molecules. The results indicate that the hydrogen-removal efficiency by bubbles does not linearly scale with increasing bubble population. Given that bubble coverage intensifies with bubble density, an optimal bubble quantity is likely to maximize overall performance. Therefore, a reasonable nucleation sites density of bubble is a crucial factor in optimizing the electrode.

Data availability

Data will be made available upon request.

Author contributions

Weikang Yang: writing-original draft, conceptualization, methodology, and data curation. Dongxu Gu: writing-review & editing. Xin Liu: investigation and writing-review & editing. Qiangming Luo: software and data curation.

Conflicts of interest

The authors declare that they have no known competing financial interests or personal relationships that could have appeared to influence the work reported in this paper.

Acknowledgements

This work was supported by the Fundamental Research Funds for the Central Universities (2023CDJXY-045), the graduate research and innovation foundation of Chongqing (CYB23014) and High-level Talent Research Start-up Project Funding of Henan Academy of Sciences (241826209).

Notes and references

1 S. Park, L. Liu, C. Demirkir, O. van der Heijden, D. Lohse, D. Krug and M. T. M. Koper, Solutal Marangoni effect determines bubble dynamics during electrocatalytic hydrogen evolution, *Nat. Chem.*, 2023, **15**, 1532–1540.
2 A. Bashkatov, S. Park, C. Demirkir, J. A. Wood, M. T. M. Koper, D. Lohse and D. Krug, Performance enhancement of electrocatalytic hydrogen evolution through coalescence-induced bubble dynamics, *J. Am. Chem. Soc.*, 2024, **146**, 10177–10186.
3 T. Dong, X. Duan, Y. Huang, D. Huang, Y. Luo, Z. Liu, X. Ai, J. Fang and C. Song, Enhancement of hydrogen production via optimizing micro-structures of electrolyzer on a microfluidic platform, *Appl. Energy*, 2024, **356**, 122376–122385.
4 J. Ryu and D. W. Lee, Tailoring hydrophilic and hydrophobic microenvironment for gas-liquid-solid triphase electrochemical reactions, *J. Mater. Chem. A*, 2024, **12**, 10012–10043.
5 J. Park, I. Cho, H. Jeon, Y. Lee, J. Zhang, D. Lee, M. K. Cho, D. J. Preston, B. Shong, I. S. Kim and W. K. Lee,

© 2025 The Author(s). Published by the Royal Society of Chemistry

Open Access Article. Published on 21 May 2025. Downloaded on 6/14/2026 1:50:35 PM. This article is licensed under a Creative Commons Attribution-NonCommercial 3.0 Unported Licence.

Conversion of layered WS_2 crystals into mixed-domain electrochemical catalysts by plasma-assisted surface reconstruction, *Adv. Mater.*, 2024, 2314031–2314042.

6 S. Hwang, H. Gu, J. L. Young, M. A. Steiner, A. B. Laursen, R. A. Crichton, Y.-W. Yeh, P. E. Batson, L. C. Feldman, M. Li, K. Wyatt, A. Safari, T. G. Deutsch, E. Garfunkel and G. C. Dismukes, TiO_2/TiN interface enables integration of Ni_5P_4 electrocatalyst with a III-V Tandem photoabsorber for stable inassisted solar-driven water splitting, *ACS Energy Lett.*, 2024, **9**, 789–797.

7 D. Wang, Y. Lian, H. Fu, Q. Zhou, Y. Zheng and H. Zhang, Flexible porous carbon nanofibers derived from cuttlefish ink as self-supporting electrodes for supercapacitors, *J. Power Sources*, 2024, **599**, 234216–234225.

8 Z. Han, H. Zhao, C. Peng, C. Fan, G. Wang, J. Zhang and Z. Tang, 3D-printed pyramid nickel-based electrode enabling directional bubble traffic and electrolyte flow for efficient hydrogen evolution, *Int. J. Hydrogen Energy*, 2024, **64**, 476–486.

9 K. Fan, L. Zong, J. Liu, C. H. Chuang, M. Dong, Y. Zou, Y. Xu, H. Q. Fu, L. Zhang, L. Wang, M. Zhou, T. Zhan, P. Liu and H. Zhao, *In situ* reconstruction to surface sulfide adsorbed metal scaffold for enhanced electrocatalytic hydrogen evolution activity, *Adv. Energy Mater.*, 2024, 2400052–2400061.

10 M. Zhong, M. Xu, S. Ren, W. Li, C. Wang, M. Gao and X. Lu, Modulating the electronic structure of $Ni(OH)_2$ by coupling with low-content Pt for boosting the urea oxidation reaction enables significantly promoted energy-saving hydrogen production, *Energy Environ. Sci.*, 2024, **17**, 1984–1996.

11 B. Wang, X. Chen, Y. He, Q. Liu, X. Zhang, Z. Luo, J. V. Kennedy, J. Li, D. Qian, J. Liu and G. I. N. Waterhouse, Fe_2O_3/P-doped $CoMoO_4$ electrocatalyst delivers efficient overall water splitting in alkaline media, *Appl. Catal., B*, 2024, **346**, 123741–123752.

12 Y. Yao, J. He, X. Zhu, L. Mu, J. Li, K. Li and M. Qu, Wettability and heterojunction synergistic interface optimization guided Co doped MoS_2/Ni_3S_2-GO/NF catalytic electrode to boost overall water splitting, *Int. J. Hydrogen Energy*, 2024, **51**, 207–221.

13 K. Wang, C. Liao, W. Wang, Y. Xiao, X. Liu and Y. Zuo, Removal of gas bubbles on an electrode using a magnet, *ACS Appl. Energy Mater.*, 2020, **3**, 6752–6757.

14 J. Das, S. Mandal, A. Borbora, S. Rani, M. Tenjimbayashi and U. Manna, Modulating force of nucleated hydrogen bubble adhesion to boost electrochemical water splitting, *Adv. Funct. Mater.*, 2023, **34**, 2311648–2311658.

15 Y. Chen, J. Chen, K. Bai, Z. Xiao and S. Fan, A flow-through electrode for hydrogen production from water splitting by mitigating bubble induced overpotential, *J. Power Sources*, 2023, **561**, 232733–232740.

16 C. H. Zhang, Z. Xu, N. Han, Y. Tian, T. Kallio, C. M. Yu and L. Jiang, Superaerophilic/superaerophobic cooperative electrode for efficient hydrogen evolution reaction via enhanced mass transfer, *Sci. Adv.*, 2023, **9**, 6978–6987.

17 Y. Zhang, W. Cui, L. Li, C. Zhan, F. Xiao and X. Quan, Effect of aligned porous electrode thickness and pore size on bubble removal capability and hydrogen evolution reaction performance, *J. Power Sources*, 2023, **580**, 233380–233387.

18 J. Bleeker, C. van Kasteren, J. R. van Ommen and D. A. Vermaas, Gas bubble removal from a zero-gap alkaline electrolyser with a pressure swing and why foam electrodes might not be suitable at high current densities, *Int. J. Hydrogen Energy*, 2024, **57**, 1398–1407.

19 H. Sarma, S. Mandal, A. Borbora, J. Das, S. Kumar and U. Manna, Self-healable, Tolerant superaerophobic coating for improving electrochemical hydrogen production, *Small*, 2024, 2309359–2309368.

20 Q. Ren, L. Feng, C. Ye, X. Xue, D. Lin, S. Eisenberg, T. Kou, E. B. Duoss, C. Zhu and Y. Li, Nanocone-Modified Surface Facilitates Gas bubble detachment for high-rate alkaline water splitting, *Adv. Energy Mater.*, 2023, **13**, 2302073–2302080.

21 M. Bae, Y. Kang, D. W. Lee, D. Jeon and J. Ryu, Superaerophobic polyethyleneimine hydrogels for improving electrochemical hydrogen production by promoting bubble detachment, *Adv. Energy Mater.*, 2022, **12**, 2201452–2201460.

22 Kirti, N. Nandha, P. S. Singh and D. N. Srivastava, Improved OER performance on the carbon composite electrode through tailored wettability, *ACS Appl. Energy Mater.*, 2021, **4**, 9618–9626.

23 J. R. Lake, A. M. Soto and K. K. Varanasi, Impact of bubbles on electrochemically active surface area of microtextured gas-evolving electrodes, *Langmuir*, 2022, **38**, 3276–3283.

24 R. Iwata, L. Zhang, K. L. Wilke, S. Gong, M. He, B. M. Gallant and E. N. Wang, Bubble growth and departure modes on wettable/non-wettable porous foams in alkaline water splitting, *Joule*, 2021, **5**, 887–900.

25 X. Lu, D. Yadav, B. Ma, L. Ma and D. Jing, Rapid detachment of hydrogen bubbles for electrolytic water splitting driven by combined effects of Marangoni force and the electrostatic repulsion, *J. Power Sources*, 2024, **599**, 234217–234227.

26 P. van der Linde, P. Peñas-López, Á. Moreno Soto, D. van der Meer, D. Lohse, H. Gardeniers and D. Fernández Rivas, Gas bubble evolution on microstructured silicon substrates, *Energy Environ. Sci.*, 2018, **11**, 3452–3462.

27 N. P. Brandon and G. H. Kelsall, Growth kinetics of bubbles electrogenerated at microelectrodes, *J. Appl. Electrochem.*, 1985, **15**, 475–484.

28 Y. Wang, X. Hu, Z. Cao and L. Guo, Investigations on bubble growth mechanism during photoelectrochemical and electrochemical conversions, *Colloids Surf., A*, 2016, **505**, 86–92.

29 X. Yang, F. Karnbach, M. Uhlemann, S. Odenbach and K. Eckert, Dynamics of single hydrogen bubbles at a platinum microelectrode, *Langmuir*, 2015, **31**, 8184–8193.

30 A. Bashkatov, X. Yang, G. Mutschke, B. Fritzsche, S. S. Hossain and K. Eckert, Dynamics of single hydrogen bubbles at Pt microelectrodes in microgravity, *Phys. Chem. Chem. Phys.*, 2021, **23**, 11818–11830.

Open Access Article. Published on 21 May 2025. Downloaded on 6/14/2026 1:50:35 PM.
This article is licensed under a Creative Commons Attribution-NonCommercial 3.0 Unported Licence.

31 A. Bashkatov, S. S. Hossain, G. Mutschke, X. Yang, H. Rox, I. M. Weidinger and K. Eckert, On the growth regimes of hydrogen bubbles at microelectrodes, *Phys. Chem. Chem. Phys.*, 2022, **24**, 26738–26752.

32 J. Qin, T. Xie, D. Zhou, L. Luo, Z. Zhang, Z. Shang, J. Li, L. Mohapatra, J. Yu, H. Xu and X. Sun, Kinetic study of electrochemically produced hydrogen bubbles on Pt electrodes with tailored geometries, *Nano Res.*, 2021, **14**, 2154–2159.

33 Z. Zhao, N. Martino, L. Tagliabue, A. Minguzzi and A. Vertova, Facile preparation of robust and multipurpose microelectrodes based on injected epoxy resin, *Electrochim. Acta*, 2023, **437**, 141454–141461.

34 M. Li, P. Xie, L. Yu, L. Luo and X. Sun, Bubble engineering on micro-/nanostructured electrodes for water splitting, *ACS Nano*, 2023, **17**, 23299–23316.

35 G. R. Seetharaman, D. N. P and J. S. Sangwai, Silica nanofluids in low salinity water for wettability alteration of the mineral surface and the effect of surface roughness, *Energ. Fuel*, 2024, **38**, 2830–2843.

36 J. Ma, M. Yang, G. Zhao, Y. Li, B. Liu, J. Dang, J. Gu, S. Hu, F. Yang and M. Ouyang, Ni electrodes with 3D-ordered surface structures for boosting bubble releasing toward high current density alkaline water splitting, *Ultrason. Sonochem.*, 2023, **96**, 106398–106405.

37 C. Park and J. Chang, Suppression of H_2 bubble formation on an electrified Pt electrode interface in an acidic "water-in-salt" electrolyte solution, *J. Mater. Chem. A*, 2022, **10**, 23113–23123.

38 C. Yu, M. Cao, Z. Dong, K. Li, C. Yu, J. Wang and L. Jiang, Aerophilic electrode with cone shape for continuous generation and efficient collection of H_2 bubbles, *Adv. Funct. Mater.*, 2016, **26**, 6830–6835.

39 X. Lu, T. Nie, X. Li, L. Jing, Y. Zhang, L. Ma and D. Jing, Insight into pH-controlled bubble dynamics on a Pt electrode during electrochemical water splitting, *Phys. Fluids*, 2023, **35**, 103314–103326.

40 X. Luo, Q. Xu, X. Ye, M. Wang and L. Guo, Mass transfer mechanism of single bubble evolution on TiO_2 electrode surface under decreased pressure, *Int. J. Hydrogen Energy*, 2024, **61**, 859–872.

41 P. Danckwerts, Significance of liquid-film coefficients in gas absorption, *Ind. Eng. Chem. Res.*, 1951, **43**, 1460–1467.

© 2025 The Author(s). Published by the Royal Society of Chemistry